Surface Turbulence Reveals Riverbed Drag Coefficient

R. A. Branch[1,2], A. R. Horner-Devine[1], C. C. Chickadel[3], S. A. Talke[4], A. T. Jessup[3], D. Clark[3]

[1]Civil and Environmental Engineering, University of Washington, Seattle, WA
[2]now at Pacific Northwest National Laboratory, Seattle, Washington, USA.
[3]Applied Physics Laboratory, University of Washington, Seattle, WA
[4]Civil and Environmental Engineering, Cal Poly, San Luis Obispo, CA

Key Points:

- Derived an equation for the drag coefficient based on the surface turbulence
- We present a field study using remotely sensed surface turbulent kinetic energy to estimate the riverbed drag coefficient
- These are the first remote measurements of the riverbed drag coefficient that have been validated with in situ measurements

Corresponding author: R. A. Branch, `Ruth.Branch@pnnl.gov`

Abstract

Flow in rivers and the coastal ocean is controlled by the frictional force exerted on the water by riverbed or seabed roughness. The frictional force is typically characterized by a drag coefficient C_d, which is estimated from bulk measurements and often assumed constant. Here we demonstrate a relationship between bed roughness and water surface turbulence that can be used to make remote estimates of C_d. We observe that regions with higher bed roughness result in higher turbulent kinetic energy (TKE), which is transported upward by river boils to the water surface. We present a relationship between surface TKE and C_d, and validate this relationship by comparing remotely-sensed estimates of C_d to those from *in situ* measurements. Thus, our results provide an approach for estimating bottom roughness and C_d based entirely on remotely sensed data, including their spatial variability, which can improve modeling of river discharge and morphodynamics in data-poor regions.

Plain Language Summary

Water flow in rivers and near the beach is controlled by the roughness of the riverbed or seabed. When water flows over the rocks, sand grains, or sand dunes on the bottom it becomes turbulent and the turbulence rises to the surface. In a river, the turbulence is in the form of boils can be observed with an infrared camera viewing the surface. We observe stronger boils over areas of the river with rough riverbeds. Here we show a mathematical equation that connects the boils observed on the water surface to the riverbed roughness and drag coefficient. Our results demonstrate that information about bottom roughness propagates upwards through the water column and therefore the drag coefficient can be estimated from remotely sensed videos of the water surface. The mathematical connection we derived between the drag coefficient and surface turbulence will be useful for improving river discharge and gas exchange models.

1 Introduction

The drag coefficient is a fundamental parameter of all boundary-layer physics problems modeling fluid flow. Numerical and analytical models of rivers, floodplains, and tidal estuaries all require estimates of a drag coefficient related to bed roughness (Godin, 1999; Wang et al., 2011; Helaire et al., 2019; Fringer et al., 2019). At present, drag coefficient measurements are needed for algorithms being developed to estimate global river flow using the satellite altimetry measurements from the upcoming Surface Water and Ocean Topography (SWOT) mission (Biancamaria et al., 2016). In practice, the drag coefficient is typically estimated from velocity measurements one meter above the riverbed (Fong et al., 2009) or from the grain size of riverbed sediment (Arcement & Schneider, 1989). A remotely-sensed estimate of the drag coefficient would circumvent the difficulty of using *in situ* measurements and would provide additional information about the spatial and temporal variability of bottom roughness.

Turbulence at the water surface can disrupt the O(1 mm) thick cool surface thermal boundary layer, or cool skin layer, which is present under conditions of net upward heat flux (Saunders, 1967). The resulting temperature anomalies can be mapped using an infrared camera and used to quantify the surface turbulence (Jessup et al., 1997). In the case of river flow, thermal signatures are produced by turbulent boils that rise to the surface after being generated by flow over a rough bottom (Chickadel et al., 2011). We collected infrared images of the surface thermal field at ten locations along a tidally influenced section of the Snohomish River (Washington, USA) and observed that the intensity of turbulent disruptions increased over river sections with large dunes and ripples. Images collected from a site with smooth bathymetry showed small boils, a streaky pattern in the flow direction, and a weak temperature anomaly that indicated gentle disruption of the cool skin layer (Fig. 1a). Images from a site with higher bottom rough-

ness showed large energetic coherent boils that disrupted the surface and caused large temperature anomalies (Fig. 1b). Sequences of these images analyzed using particle imaging velocimetry (PIV) provide the surface velocity and turbulence statistics (Chickadel et al., 2011) that are necessary to characterize the turbulence. We investigate the relationship between bottom-generated turbulence and its surface manifestation, providing a framework for the use of remotely-sensed turbulence statistics to quantify the bottom drag coefficient, C_d.

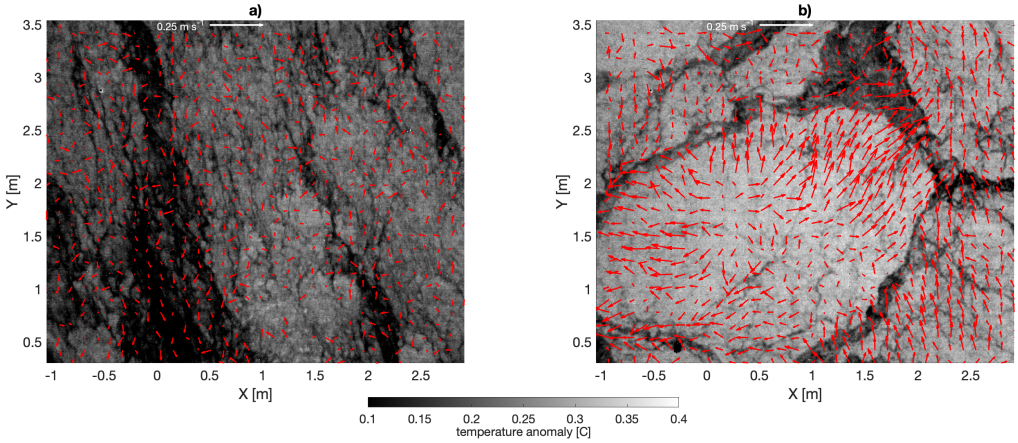

Figure 1. Infrared images from two sites with similar flow velocities but different riverbed roughness values and surface turbulence. The colorscale is the temperature anomaly relative to the coolest temperature in the image (dark = cool; bright = warm). Arrows show velocity. a) site E2: $u = 0.75$ m/s, $H = 2.68$ m, $C_d = 0.0013$ b) site E5: $u = 0.75$ m/s, $H = 2.64$ m, $C_d = 0.0086$. A movie of the water surface is provided in the Supplementary Information.

Turbulent velocity fluctuations have been predicted to decrease exponentially between the bed and the surface and to increase with roughness during steady flow with a logarithmic velocity profile (Nezu & Nakagawa, 1993). The resulting three equations predicting this behavior have been tested in laboratory experiments and shown to correctly describe the vertical profiles of the horizontal (u'_{rms}, v'_{rms}) and vertical (w'_{rms}) components of the velocity fluctuations in a wide channel, regardless of the Froude or Reynolds numbers (Auel et al., 2013). This suggests that these equations could be used to relate bottom roughness to surface turbulence. We have used these three equations to derive a single equation for the turbulent kinetic energy:

$$TKE = 4.78u_*^2 exp(-2\frac{z}{H}). \tag{1}$$

where u_* is the friction velocity, z is the height above the bed, H is the water depth, and the turbulent kinetic energy is defined as $TKE = 1/2({u'_{rms}}^2 + {v'_{rms}}^2 + {w'_{rms}}^2)$. The drag coefficient, C_d, is also dependent on u_* and is defined as

$$C_d = \frac{u_*^2}{u^2}. \tag{2}$$

where u is the flow velocity (Sanford & Lien, 1999). With $\frac{z}{H} = 1$ at the surface, equation (1) can be solved for u_*, which is then substituted into (2) to give

$$C_d = \frac{TKE_{surface}}{0.65u^2}. \tag{3}$$

This equation relates the roughness-induced bottom drag directly to the normalized surface TKE. The normalized surface TKE and the surface velocity can be measured remotely using infrared imagery. The surface velocity is expected to be higher than the velocity one meter above the bed traditionally used in equation (2), therefore C_d calculated with the surface velocity is an approximation for C_d measured near the bed. The validity of this approximation is discussed in the Supplemental Information. The lack of dependence on depth in this equation is surprising. While it is true that deep sections of a river have less surface TKE, this is due to the fact that the flow slows down as it encounters a larger cross-sectional area. For two sections of river with similar velocities, still waters indicate a smooth riverbed.

2 Observations

The Coherent Structures Experiment, (COHSTREX), collected surface and water column velocity and turbulence data at ten sites on a tidal section of the Snohomish River in September 2009 (Talke et al., 2013; Chickadel et al., 2011).

We used multibeam sonar surveys to map the bathymetry and bottom roughness at the experiment site. The total Nikuradse roughness, k, was calculated as the sum of the grain size, D_{90}, and the primary and secondary dune roughness values (Jellesma, 2013). The primary and secondary dune roughness values are given by $k''_{N,p} = 1.1\delta_p(1-e^{-25\delta_p/\lambda_p})$ and $k''_{N,s} = 1.1\delta_s(1-e^{-25\delta_s/\lambda_s})$ where δ is the dune height, λ is the dune length, p stands for primary, and s stands for secondary. The primary and secondary peaks of a bathymetry transect spectrum are shown for site F3 in Fig. 2l. Nearby historical surveys showed a grain size of one mm (DeVries, 2015), which was used as the D_{90}. Site F4 (Fig. 2h) was excluded from the analysis because the bathymetry transect did not have repeating sinusoidal bedforms. We used spectral analysis of multiple bathymetric profiles at each site to derive the dune height and length parameters required for calculating k and its error bars (Fig. 2l).

Surface velocity measurements were made using PIV techniques applied to infrared imagery(Chickadel et al., 2011). Spectra were calculated using three minute sections of the data and fit to $f^{-5/3}$ between 0.1 and 2 Hz. The R^2 of the fit was used to determine whether the data should be used to calculate C_d. A good spectral fit to $f^{-5/3}$ indicated that the turbulence was consistent with the energy cascade from large to small scales (Kundu et al., 2015), whereas a fit with a low R^2 value indicated either that it was early in the tide and the turbulent field was not fully developed, or that noisy imagery or surface waves corrupted the spectra. Surface velocity measurements were excluded when the flow was unsteady and the depth averaged acceleration measured by the ADCP was greater than 0.1 m/s^2. The surface kinematic boundary condition requires that $w = 0$ at the surface and the energy from w'_{rms} is transferred to u'_{rms} and v'_{rms} (Shen et al., 1999). The surface turbulent kinetic energy measured with infrared imagery, $TKE_{surface} = 1/2({u'_{rms}}^2 + {v'_{rms}}^2)$, was used in equation (3) to calculate C_d. Infrared imagery was collected at all ten sites but only six had usable data for the C_d calculation.

We measured *in situ* velocities with a downward-facing four-beam ADCP at one Hz in 0.25 m depth bins from the river bottom up to 1.5 m below the surface (Talke et al., 2013). Reynolds stresses ($\overline{u'w'}$) and the three components of velocity (u, v, w) were computed from the ADCP data following the methods of Stacey, Monismith, and Burau (1999). The drag coefficient was computed based on *in situ* data as the slope of a linear fit between $\overline{u'w'}$ and $u\sqrt{u^2+v^2}$ (Figure 3a), where the velocities are measured one meter above the bed (Sanford & Lien, 1999; Fong et al., 2009).

Salinity was measured continuously with conductivity temperature depth instruments (CTDs) on the riverbed and at the surface to monitor for periods of decreased surface turbulence due to tidal intrusion of the salt wedge (Beuzen et al., 2016). The re-

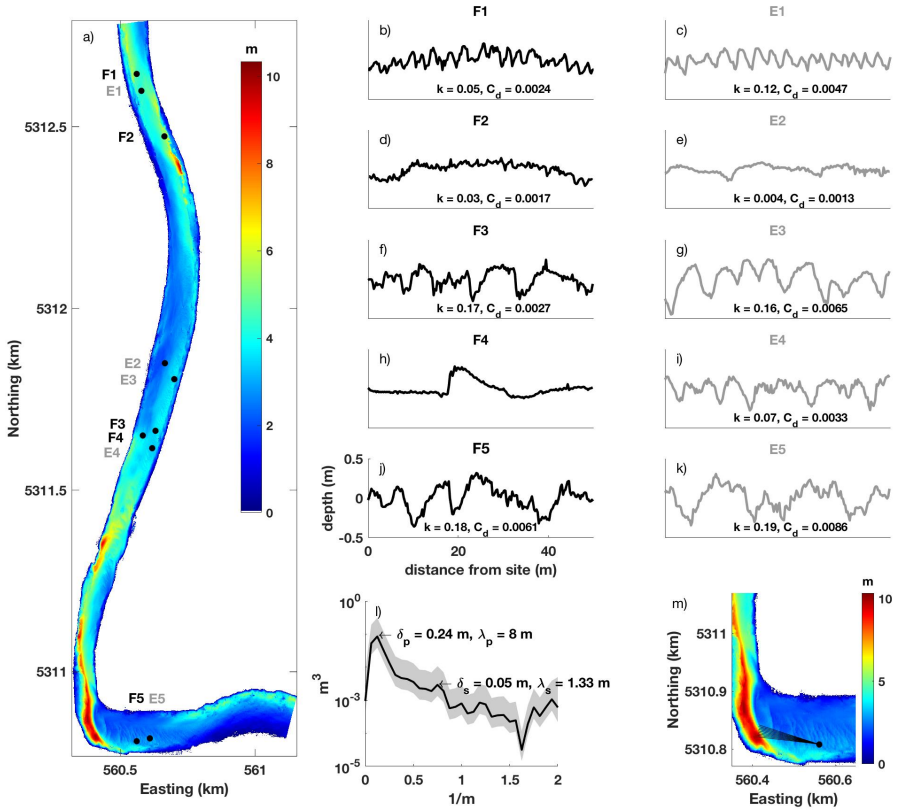

Figure 2. Snohomish riverbed roughness a) Multibeam sonar survey showing five ebb (E1-E5) and five flood (F1-F5) tide sites. Flow direction is from top to bottom during flood tide and bottom to top during ebb tide. b-k) fifty-meter transects of the bathymetry upstream of the sites. Flow direction is from right to left. Nine sites are marked with k values calculated using sonar scan data and C_d values calculated using velocity data measured one meter above the bed (mab). l) Example power spectrum of the F3 bathymetry transect showing the primary and secondary dune heights, δ, and lengths, λ. The shading shows the 95% confidence interval of the spectrum. m) Nine bathymetry transects extracted from site E5 showing a span of nine degrees.

motely sensed surface data used in the C_d calculations were acquired when the salinity difference between the surface and bed measurements was less than 0.5 PSU.

3 Analysis and Results

Riverbed roughness varies substantially between the ten study sites (Fig. 2). The roughness at most of the sites is characterized as either periodic dunes (F1, E1, E3, and F3) or non-periodic large-scale features with small-scale roughness (F2, E2, and F4). The dune heights ranged from 0.01 to 0.36 m and the dune lengths ranged from 0.66 to 16 m, resulting in a Nikuradse roughness length range of $k = 0.004$ to $k = 0.19$ (Fig. 2b-k). We found that k is sensitive to the angle between the bathymetry transect and the main flow direction for sections of the river where the cross-stream bathymetry is not uniform. For example, transects that included large deviations, such as a deep hole (Figure 2m), had larger error bars on k than those that did not.

The drag coefficient was calculated following the methods of using Sanford and Lien (1999); Fong et al. (2009) and is illustrated in Figure 3a, where the velocities are measured one meter above the bed. This analysis was repeated at all nine sites for twenty tidal measurement periods and shows a strong correlation between C_d computed from the *in situ* data and k (Figure 3b). The site-averaged C_d values range from 0.0013 to 0.0086 and the robust linear fit to the average C_d versus k has an R^2 of 0.93. This confirms that our measurements capture the relationship between near-bed turbulence and bed roughness, and that the turbulence is adequately parameterized by the drag coefficient. In order to be detectable on the water surface, the roughness dependence observed in near-bed turbulence must also be apparent higher in the water column. This is confirmed in Figure 3c, where we plot profiles of normalized TKE for three sites spanning a range of roughness. Sites with higher k values had larger normalized TKE both near the bottom and throughout the water column; thus, the TKE signal of riverbed roughness propagates from the bottom to the surface.

In Figure 4 we show that remotely-derived values of the drag coefficient have a strong relationship to k over the full range of values of bottom roughness. The values of C_d are calculated using measurements of TKE and u from PIV at the surface via equation (3) and k is calculated as described in Section 2. The remotely-sensed values of C_d also show remarkable agreement with the C_d estimates based on *in situ* velocity. The average difference between the surface TKE and the *in situ* estimates of C_d is 0.0007 with a standard deviation of 0.0016. The strong correlation between the remotely-estimated drag coefficient and the bottom roughness, and the excellent agreement between the two independent methods of estimating C_d provide strong evidence for the validity of equation (3).

4 Discussion

Our results demonstrate a new technique for remote spatial mapping of C_d, allowing for convenient tracking of changes in bottom roughness over both time and space to improve predictions of river flow and coastal floods. Remotely measured drag coefficient values are similar in magnitude to values measured with *in situ* instruments, and also compare well with estimates from prior *in situ* measurements (Fong et al., 2009; Li et al., 2004) and modeling studies (Kukulka & Jay, 2003; Ralston et al., 2019). Our C_d estimates vary by more than a factor of three within a 2 km section of the river, emphasizing the potential importance of resolving the spatial variability of roughness for accurately modeling river turbulence and flow.

We observe a strong relationship between riverbed roughness and C_d based on surface TKE (Fig. 4) despite the fact that these measurements include a factor of two variation in depth that is not accounted for in the current formulation of C_d from water sur-

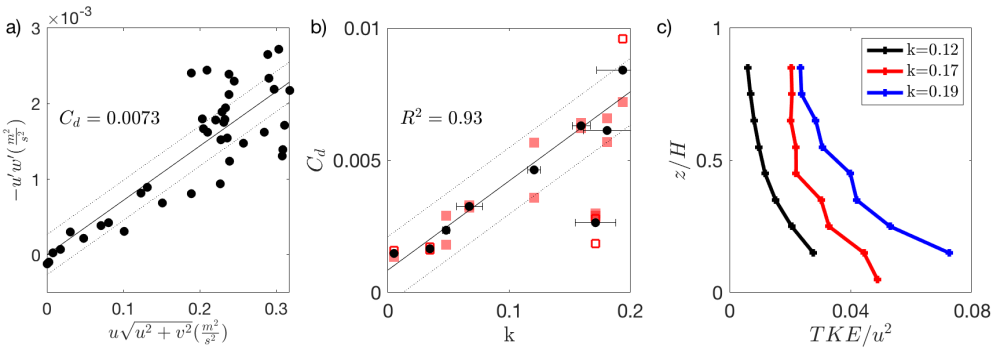

Figure 3. Calculation of C_d using ADCP data one mab a) Example calculation of C_d for one tide at site E5 based on *in situ* data. Dashed lines: 95% confidence interval. b) C_d calculated for twenty tides at all nine sites from *in situ* data plotted versus k derived from bathymetry. Red squares are the measurements at each tide and black circles are the average C_d for each site. Error bars are the standard error of nine k values calculated from bathymetry transects spanning nine degrees (example shown in Fig. 1m). Filled squares are tides where the fit to determine C_d had $R^2 > 0.5$ and open squares are where $R^2 < 0.5$. The black line is a robust fit to the site averages and the dashed lines are 95% confidence intervals. The outlier in the lower right (F3) had four tides, two of which had C_d fit with $R^2 < 0.5$. c) Vertical profiles of normalized TKE for three sites with different k values.

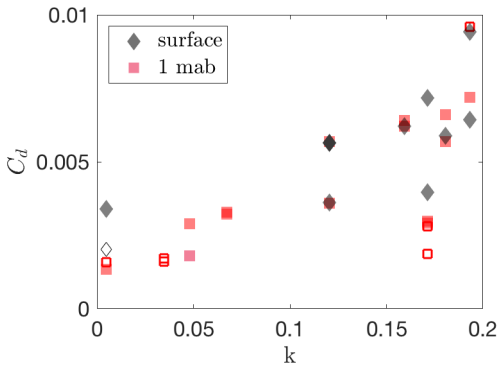

Figure 4. C_d versus k measured with surface infrared imagery and 1 m above the bed (repeated from Fig. 3b). The open diamond indicates that the R^2 of the fit of the infrared velocity spectra to $f^{-5/3}$ was above 0.88, and filled diamonds indicate that the R^2 was above 0.9. Filled squares are data points where the ADCP C_d fit had an $R^2 > 0.5$, and open squares are where $R^2 < 0.5$. The outlier in the lower right (F3) is the same as noted in Fig. 3b. Here the remotely sensed C_d value is higher and closer to the overall trend.

face measurements (Equation 3). We conclude that depth dependence is secondary for the range of depths observed in our experiments, which are typical of river and estuarine systems. However, surface TKE would likely depend on depth in a very deep river or estuary where bottom generated turbulence may not propagate all the way to the surface. Those conditions would not have a logarithmic velocity profile that was required in our derivation.

5 Summary

Our measurements show that the imprint of bottom generated turbulence is detectable on the water surface, allowing bottom roughness to be determined based on remote measurements of turbulence on the surface. We quantify turbulence at the water surface in terms of a drag coefficient C_d, according to Equation 3, which is derived based on assumptions of steady, uniform flow, an exponential turbulence profile and a logarithmic velocity profile. Bed roughness is quantified in terms of roughness height k, which is shown to be a good predictor of surface turbulence. Equation 3 can also be used to estimate TKE when C_d and u are available, e.g., from local sediment samples and river gauges, respectively. Since gas transfer can be parameterized by TKE (Zappa et al., 2007), our results may also help to improve global estimates of riverine carbon fluxes, which are currently poorly estimated (Allen & Pavelsky, 2018).

6 Supplementary Materials

6.1 Video

Video of infrared images with PIV vectors showing the velocity for the two sites shown in Fig. 1. The video has been slowed to half speed. (BoilsRiverbedRoughness.avi).

6.2 Derivations

The drag coefficient is defined (Sanford & Lien, 1999) as $C_d = \frac{u_*^2}{u_{1mab}^2}$, but often calculated (Sanford & Lien, 1999; Fong et al., 2009) as $C_d = \frac{\overline{u'w'}}{u_{1mab}^2}$ using *in situ* measurements. Our calculations of C_d from remotely sensed data use u_*^2 calculated from surface TKE and $u_{surface}$ where $u_{surface}$ is an approximation for u_{1mab}. Our calculations of C_d from *in situ* data approximate the bed stress with $\overline{u'w'}$ measured one meter above the bottom, which is an assumption of a constant stress layer in the bottom meter of water. Here we explain the conditions under which we would expect the remotely sensed and *in situ* C_d values to agree as they have for our experiment.

Our derivation is based on the assumption of a logarithmic velocity profile, which can be written as

$$u(z) = \frac{u_*}{\kappa} ln \frac{z}{z_0} \tag{4}$$

where κ is ≈ 0.41 and z_0 is the roughness height. A logarithmic velocity profile implies $u_{surface} > u_{1mab}$ and equation (3) should account for this difference as

$$C_d = \frac{TKE_{surface}}{0.65 u_{1mab}^2} = \frac{TKE_{surface} r^2}{0.65 u_{surface}^2} \tag{5}$$

where $r = \frac{u_{surface}}{u_{1mab}}$. Thus neglecting the r^2 would cause an underestimation of C_d yet the values we calculate agree remarkably well with those measured with *in situ* data.

Our calculation of C_d from *in situ* data relies on the approximation that $u_*^2 = \overline{u'w'}$ where $\overline{u'w'}$ is measured one meter above the bed instead of at the bed. If $\overline{u'w'}$ one meter above the bed is larger than $\overline{u'w'}$ at the bed then our calculation of C_d would be underestimated. Although C_d is often calculated using $\overline{u'w'}$ measured one meter above the bed, this is an approximation to be used when $z/H \approx 0$ due to $z = 1$ and a large H value. The formula for u_*^2 is given as(Nezu & Nakagawa, 1993)

$$u_*^2 = \frac{\overline{u'w'}}{1 - \frac{z}{H}} \tag{6}$$

This formula is derived from continuity and Navier-Stokes for 2-D open channel flow as:

$$u\frac{\partial u}{\partial x} + w\frac{\partial u}{\partial z} = gsin\theta - \frac{\partial}{\partial x}\left(\frac{P}{\rho}\right) + \frac{\partial}{\partial x}(-\overline{u^2}) + \frac{\partial}{\partial z}(-\overline{u'w'}) + \nu\nabla^2 u \tag{7}$$

and

$$u\frac{\partial w}{\partial x} + w\frac{\partial w}{\partial z} = -gcos\theta - \frac{\partial}{\partial x}\left(\frac{P}{\rho}\right) + \frac{\partial}{\partial x}(-\overline{u'w'}) + \frac{\partial}{\partial z}(-\overline{w^2}) + \nu\nabla^2 w \tag{8}$$

where P is the pressure, ρ is the density of water, and ν is the viscosity. For uniform open-channel flow where $w = 0$ and $\frac{\partial}{\partial x} = 0$, equation (8) is integrated in the z direction to give:

$$\frac{P}{\rho} = (H - z)gcos\theta + (w_s'^2 - w'^2) \tag{9}$$

where w_s' is the magnitude of the vertical fluctuations of w at the surface, which goes to zero due to the free surface condition. Equations (7) and (9) can be combined to give

$$\frac{\tau}{\rho} = \overline{u'w'} + \nu\frac{\partial u}{\partial z} = u_*^2\left(1 - \frac{z}{H}\right). \tag{10}$$

When viscosity is negligible, $u_*^2 = \frac{\overline{u'w'}}{(1-\frac{z}{H})}$ which can be substituted into $C_d = \frac{u_*^2}{u_{1mab}^2}$ to give

$$C_d = \frac{\overline{u'w'}}{(1 - \frac{z}{H})u_{1mab}^2}. \tag{11}$$

When $\frac{z}{H} \approx 0$, the equation for C_d measured with *in situ* data becomes

$$C_d = \frac{\overline{u'w'}}{u_{1mab}^2}. \tag{12}$$

The remotely sensed C_d values calculated with the $u_{surface} \approx u_{1mab}$ will agree well with the *in situ* C_d values calculated with the $\frac{z}{H} \approx 0$ approximation when

$$r^2 \approx \frac{1}{1 - \frac{z}{H}}. \tag{13}$$

The logarithmic velocity profile implies $r = \frac{ln\frac{H}{z_0}}{ln\frac{1}{z_0}}$. For an *in situ* measurement at $z = 1m$, equation (13) can be solved algebraically to give

$$ln(H)\sqrt{1 - \frac{1}{H}} \approx 1. \tag{14}$$

Figure 4 shows the condition is close to 1 for the depths of our experiment (3-6 m). When

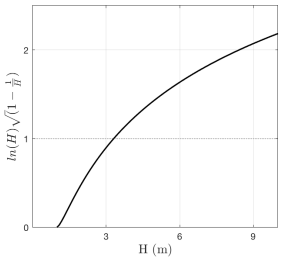

Figure 5. Two approximations will yield equivalent C_d values for depths where $ln(H)\sqrt{1 - \frac{1}{1/H}} \approx 1$.

the depth is above 9 m the condition is above 2, which implies the accuracy of C_d calculated with the $u_{surface} \approx u_{1mab}$ approximation will be small. When the depth is below 3 m the curve shown in Figure 5 falls off rapidly, also implying the accuracy of a remotely sensed C_d would be small. For depths above 9 m and below 3 m an estimate of u_{1mab} would be needed for the drag coefficient calculation.

Acknowledgments

The authors would like to the APL Marine Operations (E. Boget, Head) for running the *R/V Henderson*, and the COHSTREX team for help acquiring the data. R. Branch was funded by the NASA NESSF. A. Horner-Devine is grateful for support from the Allan and Inger Osberg Endowed Professorship, OCE-1459051, and OCE-1233068. The COHSTREX experiment was funded by a MURI grant from the Office of Naval Research (ONR), award N00014-05-0485, and ONR grand N00014-12-1-0219. Experimental data can be found at this site (https://doi.org/10.5281/zenodo.4396346).

References

Allen, G. H., & Pavelsky, T. M. (2018). Global extent of rivers and streams. *Science*, *361*(6402), 585–588.

Arcement, G. J., & Schneider, V. R. (1989). *Guide for selecting manning's roughness coefficients for natural channels and flood plains.* US Government Printing Office Washington, DC.

Auel, C., Albayrak, I., & Boes, R. M. (2013). Turbulence characteristics in supercritical open channel flows: effects of froude number and aspect ratio. *Journal of Hydraulic Engineering*, *140*(4), 04014004.

Beuzen, T., Chickadel, C. C., & Horner-Devine, A. R. (2016). Influence of subsurface stratification on turbulence and aeration in a tidal river. *IEEE Geoscience and Remote Sensing Letters*, *13*(12), 1975–1978.

Biancamaria, S., Lettenmaier, D. P., & Pavelsky, T. M. (2016). The swot mission and its capabilities for land hydrology. In *Remote sensing and water resources* (pp. 117–147). Springer.

Chickadel, C. C., Talke, S. A., Horner-Devine, A. R., & Jessup, A. T. (2011). Infrared-based measurements of velocity, turbulent kinetic energy, and dissipation at the water surface in a tidal river. *IEEE Geoscience and Remote Sensing Letters*, *8*(5), 849–853.

DeVries, P. (2015, 02). *Reach Scale Geomorphic Analysis of Hydraulic, Hydrologic, and Sediment Conditions in the Snohomish River Between SR 522 and Ebey Slough* (Tech. Rep.). R2 Resource Consultants.

Fong, D. A., Monismith, S. G., Stacey, M. T., & Burau, J. R. (2009). Turbulent stresses and secondary currents in a tidal-forced channel with significant curvature and asymmetric bed forms. *Journal of Hydraulic Engineering*, *135*(3), 198–208.

Fringer, O. B., Dawson, C. N., He, R., Ralston, D. K., & Zhang, Y. J. (2019). The future of coastal and estuarine modeling: Findings from a workshop. *Ocean Modelling*, 101458.

Godin, G. (1999). The propagation of tides up rivers with special considerations on the upper saint lawrence river. *Estuarine, Coastal and Shelf Science*, *48*(3), 307–324.

Helaire, L. T., Talke, S. A., Jay, D. A., & Mahedy, D. (2019). Historical changes in lower columbia river and estuary floods: a numerical study. *Journal of Geophysical Research: Oceans*.

Jellesma, M. (2013). *Form drag of subaqueous dune configurations* (Unpublished master's thesis). University of Twente.

Jessup, A., Zappa, C., Loewen, M., & Hesany, V. (1997). Infrared remote sensing of breaking waves. *Nature*, *385*(6611), 52.

Kukulka, T., & Jay, D. A. (2003). Impacts of columbia river discharge on salmonid habitat: 2. changes in shallow-water habitat. *Journal of Geophysical Research: Oceans*, *108*(C9).

Kundu, P. K., Dowling, D. R., Tryggvason, G., & Cohen, I. M. (2015). Fluid mechanics.

Li, C., Valle-Levinson, A., Atkinson, L. P., Wong, K. C., & Lwiza, K. M. (2004). Estimation of drag coefficient in james river estuary using tidal velocity data from a vessel-towed adcp. *Journal of Geophysical Research: Oceans*, *109*(C3).

Nezu, I., & Nakagawa, H. (1993). Turbulence in open-channel flows, iahr monograph series. *AA Balkema, Rotterdam*, 1–281.

Ralston, D. K., Talke, S., Geyer, W. R., Al-Zubaidi, H. A., & Sommerfield, C. K. (2019). Bigger tides, less flooding: Effects of dredging on barotropic dynamics in a highly modified estuary. *Journal of Geophysical Research: Oceans*, *124*(1), 196–211.

Sanford, T. B., & Lien, R.-C. (1999). Turbulent properties in a homogeneous tidal bottom boundary layer. *Journal of Geophysical Research: Oceans*, *104*(C1), 1245–1257.

Saunders, P. M. (1967). The temperature at the ocean-air interface. *Journal of the Atmospheric Sciences*, *24*(3), 269–273.

Shen, L., Zhang, X., Yue, D. K., & Triantafyllou, G. S. (1999). The surface layer for free-surface turbulent flows. *Journal of Fluid Mechanics*, *386*, 167–212.

Stacey, M. T., Monismith, S. G., & Burau, J. R. (1999). Measurements of reynolds stress profiles in unstratified tidal flow. *Journal of Geophysical Research: Oceans*, *104*(C5), 10933–10949.

Talke, S. A., Horner-Devine, A. R., Chickadel, C. C., & Jessup, A. T. (2013). Turbulent kinetic energy and coherent structures in a tidal river. *Journal of Geophysical Research: Oceans*, *118*(12), 6965–6981.

Wang, B., Giddings, S., Fringer, O., Gross, E., Fong, D., & Monismith, S. (2011). Modeling and understanding turbulent mixing in a macrotidal salt wedge estuary. *Journal of Geophysical Research: Oceans*, *116*(C2).

Zappa, C. J., McGillis, W. R., Raymond, P. A., Edson, J. B., Hintsa, E. J., Zemmelink, H. J., ... Ho, D. T. (2007). Environmental turbulent mixing controls on air-water gas exchange in marine and aquatic systems. *Geophysical Research Letters*, *34*(10).